A&A 556, A20 (2013)
DOI: 10.1051/0004-6361/201220824

Astronomy & Astrophysics

Variable stars in the globular cluster NGC 7492⋆,⋆⋆

New discoveries and physical parameter determination

R. Figuera Jaimes[1,2], A. Arellano Ferro[3], D. M. Bramich[1], S. Giridhar[4], and K. Kuppuswamy[4]

[1] European Southern Observatory, Karl-Schwarzschild-Straβe 2, 85748 Garching bei München, Germany
e-mail: rfiguera@eso.org, robertofiguera@gmail.com, dan.bramich@hotmail.co.uk
[2] SUPA, School of Physics and Astronomy, University of St. Andrews, North Haugh, St Andrews, KY16 9SS, UK
[3] Instituto de Astronomía, Universidad Nacional Autónoma de México, Apdo. Postal 70-264, México D. F. CP 04510, México
e-mail: armando@astro.unam.mx
[4] Indian Institute of Astrophysics, Bangalore, India

Received 30 November 2012 / Accepted 20 May 2013

ABSTRACT

Aims. We have performed a photometric V, R, I CCD time-series analysis with a baseline of about eight years of the outer-halo globular cluster NGC 7492 with the aim of searching for new variables and using these (and the previously known variables) to determine the physical parameters of interest for the cluster (e.g. metallicity, absolute magnitude of the horizontal branch, distance, etc.).
Methods. We used difference image analysis to extract precise light curves in the relatively crowded star field, especially towards the densely populated central region. Several different approaches were used for variability detection that recover the known variables and lead to new discoveries. We determined the physical parameters of the only RR0 star using a light-curve Fourier decomposition analysis.
Results. We found one new long-period variable and two SX Phe stars in the blue straggler region. We also present one candidate SX Phe star that requires follow-up observations. Assuming that the SX Phe stars are cluster members and using the period-luminosity relation for these stars, we estimate their distances as ∼25.2 ± 1.8 and 26.8 ± 1.8 kpc, and identify their possible modes of oscillation. We refined the periods of the two RR Lyrae stars in our field of view. We found that the RR1 star V2 is undergoing a period change and possibly exhibits the Blazhko effect. A Fourier decomposition of the light curve of the RR0 star V1 allowed us to estimate a metallicity of $[Fe/H]_{ZW} \sim -1.68 \pm 0.10$ or $[Fe/H]_{UVES} \sim -1.64 \pm 0.13$, a log-luminosity $\log(L/L_{\odot}) \sim 1.76 \pm 0.02$, an absolute magnitude $M_V \sim 0.38 \pm 0.04$ mag, and a true distance modulus of $\mu_0 \sim 16.93 \pm 0.04$ mag, which is equivalent to a distance of ∼24.3 ± 0.5 kpc. All of these values are consistent with previous estimates in the literature.

Key words. globular clusters: individual: NGC 7492 – stars: variables: RR Lyrae – blue stragglers – stars: abundances – stars: distances – stars: horizontal-branch

1. Introduction

The potential of difference image analysis (DIA) as a powerful tool for unveiling short-period variable stars or small amplitude variations in Blazhko RR Lyraes in the densely populated central regions of globular clusters (GC) has been demonstrated in recent papers (e.g. Kains et al. 2012; Arellano Ferro et al. 2012, 2011; Bramich et al. 2011; Corwin et al. 2006; Strader et al. 2002, etc.). Multi-colour time-series CCD photometry allows the identification of variable stars in specific regions of the colour–magnitude diagram (CMD). The Fourier decomposition of RR Lyrae light curves enables us to derive stellar parameters. In the blue straggler region, SX Phe stars are often found, and depending on the number of them in the cluster, their period-luminosity (P-L) relation can be calibrated or can be used to obtain an independent estimate of the distance to the cluster.

In the present paper we focus on the globular cluster NGC 7492. This is a sparse outer-halo cluster ($R_{GC} \sim 25$ kpc; Harris 1996, 2010 edition) for which detailed spectroscopic abundances exist ([Fe/H] ∼ −1.8) for four stars at the tip of the red giant branch (RGB; Cohen & Melendez 2005). Hence the cluster offers a good opportunity of comparing the spectroscopic results with the metallicity derived from the light-curve Fourier-decomposition approach for RR Lyrae stars. According to the Catalogue of Variable Stars in Globular Clusters (CVSGC; Clement et al. 2001), only four variable stars are known in this cluster; one RR0 (V1), discovered by Shapley (1920), two RR1 (V2 and V3), and one long-period variable (LPV; V4), all discovered by Barnes (1968). Although Buonanno et al. (1987) suggested the presence of a population of blue stragglers in this cluster and numerous blue stragglers have been identified by Cote et al. (1991), no investigation into the variability of these otherwise faint stars ($V \sim 20$ mag) has been reported. Taking advantage of our time-series CCD photometry of the cluster and our capability of performing precise photometry via DIA, we explored the field of the cluster for new variables.

In Sect. 2 we describe the observations, data reduction, and transformation of the photometry to the Johnson-Kron-Cousins standard system. In Sect. 3 we present a detailed discussion of the strategies employed to identify new variables. In Sect. 4 the physical parameters of the RR0 star as derived from the Fourier decomposition of its light curve and the Blazhko effect for the RR1 star are discussed. In Sect. 5, we briefly comment on the

⋆ Based on observations collected at the Indian Astrophysical Observatory, Hanle, India.
⋆⋆ Full Table 3 is available at the CDS via anonymous ftp to cdsarc.u-strasbg.fr (130.79.128.5) or via http://cdsarc.u-strasbg.fr/viz-bin/qcat?J/A+A/556/A20

Table 1. Distribution of observations of NGC 7492 for each filter.

Date	N_V[a]	t_V(s)[b]	N_R[a]	t_R(s)[b]	N_I[a]	t_I(s)[b]
20041004	7	60–200	7	150–180	–	–
20041005	16	60–120	14	100	–	–
20060801	8	120	7	100	–	–
20070804	6	240	7	100–180	–	–
20070805	4	240	3	120–180	–	–
20070904	8	180–240	8	120–180	–	–
20070905	8	180	8	120	–	–
20090107	4	100	–	–	5	100–300
20090108	5	300	–	–	5	220–300
20120628	37	90–180	–	–	–	–
20120629	16	200	–	–	–	–
TOTAL:	119		54		10	

Notes. [(a)] N_V, N_R, and N_I are the number of images taken for the filters V, R, and I. [(b)] t_V, t_R, and t_I are the exposure times, or range of exposure times, employed during each night for each filter.

long-term variables. In Sect. 6 we present a discussion for the newly found SX Phe stars and candidates, and in Sect. 7 we summarize our results.

2. Observations and reductions

The observations employed in the present work were obtained using the Johnson-Kron-Cousins V, R, and I filters on the dates listed in Table 1. We used the 2.0 m telescope of the Indian Astronomical Observatory (IAO) at Hanle, India, located at 4500 m above sea level. The typical seeing was ∼1.3 arcsec. The detector was a Thompson CCD of 2048 × 2048 pixels with a pixel scale of 0.296 arcsec/pix and a field of view of ∼10.1×10.1 arcmin^2. However, for this cluster we can only apply DIA to smaller images that cover an area of ∼6.4 × 5.5 arcmin^2 centred on the cluster because of a lack of sources towards the detector edges for use in the kernel solutions. Our data set consists of 119 images in V, 54 images in R, and 10 images in I.

The images were calibrated via standard overscan bias level and flat-field correction procedures, and DIA was performed with the aim of extracting high-precision time-series photometry of the stars in the field of NGC 7492. We used the `DanDIA`[1] pipeline for the data reduction process, which models the convolution kernel matching the point-spread function (PSF) of a pair of images of the same field as a discrete pixel array (Bramich 2008; Bramich et al. 2013). A brief summary of the `DanDIA` pipeline can be found in Arellano Ferro et al. (2011), while a detailed description of the procedure and its caveats is available in Bramich et al. (2011).

The reference image for each filter was constructed by registering and stacking the best-seeing-calibrated images such that all images used were taken on a single night. This resulted in 2, 4, and 1 images being stacked with total exposure times of 120, 400, and 100 s for the filters V, R, and I, respectively.

The light curve data in all three filters for all of the variable stars are provided in Table 3. In addition to the star magnitudes, we supply the difference fluxes $f_{\rm diff}(t)$ (ADU/s), the reference flux $f_{\rm ref}$ (ADU/s), and the photometric scale factor $p(t)$ at time t, as provided by the `DanDIA` pipeline. These quantities are linked

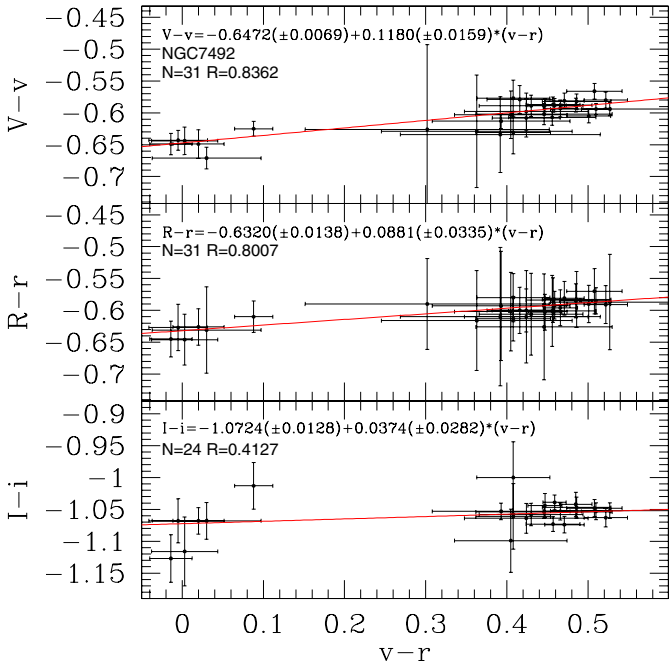

Fig. 1. Photometric transformation relations between the instrumental v, r, i and the standard V, R, I magnitudes using the standard stars from Stetson (2000).

to the instrumental magnitudes $m_{\rm ins}$ via the equations

$$f_{\rm tot}(t) = f_{\rm ref} + \frac{f_{\rm diff}(t)}{p(t)} \quad (1)$$

$$m_{\rm ins}(t) = 25.0 - 2.5\log(f_{\rm tot}(t)). \quad (2)$$

2.1. Transformation to the VRI standard system

The instrumental v, r, i, magnitudes were converted to the Johnson-Kron-Cousins photometric system (Landolt 1992) by using the standard stars in the field of NGC 7492. The V, R, and I standard stars and their magnitudes are available in the catalogue of Stetson (2000)[2]. Figure 1 displays the relations between the instrumental and standard magnitude systems as a function of instrumental $(v - r)$ colour, where we found mild colour dependencies. The standard stars have a colour range between $-0.02 < V - R < 0.53$ mag and $0.02 < V - I < 1.10$ mag, which covers the range of colours of the stars in our field of view. To convert the instrumental magnitudes into standard magnitudes for the stars without an instrumental $v - r$ colour, we assumed a value of $v - r = 0.286$ mag corresponding to the centre of the spread of instrumental $v - r$ star colours.

2.2. Astrometry and finding chart

We fitted a linear astrometric solution derived for the V filter reference image by matching 37 hand-picked stars with the UCAC3 star catalogue (Zacharias et al. 2010) using a field overlay in the image display tool GAIA (Draper 2000). We achieved a radial rms scatter in the residuals of ∼0.24 arcsec, which is equivalent to ∼0.82 pixels. To facilitate the identification of the variable stars in this cluster in future studies, we have produced a finding chart, which we present in Fig. 2. In addition, in Table 2 we

[1] `DanDIA` is built from the DanIDL library of IDL routines available at `http://www.danidl.co.uk`

[2] `http://www3.cadc-ccda.hia-iha.nrc-cnrc.gc.ca/community/STETSON/standards`

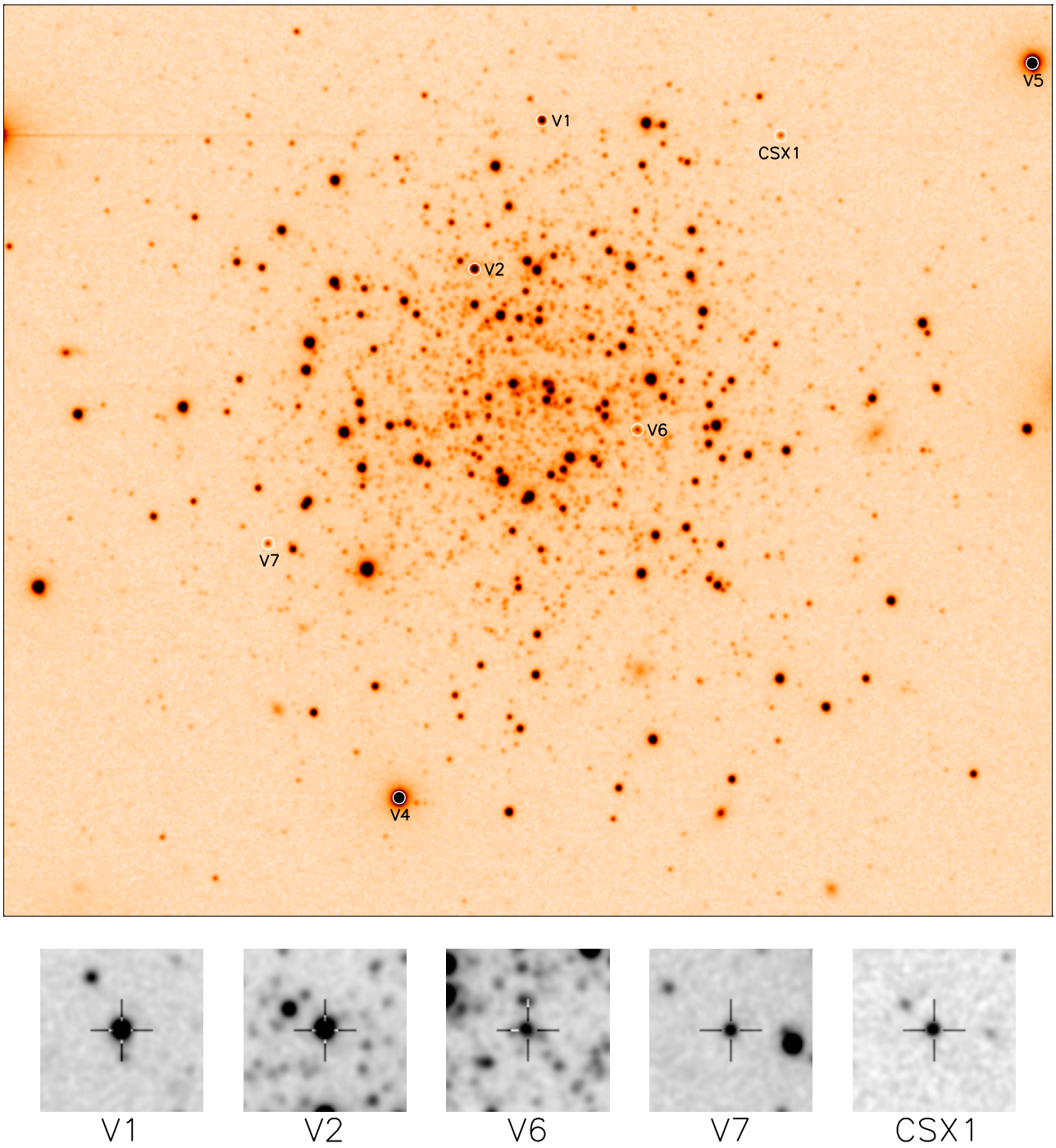

Fig. 2. Finding charts constructed from our V reference image; north is up and east is to the right. The cluster image is 6.36×5.52 arcmin^2, and the image stamps are of size 23.7×23.7 arcsec^2. Each variable (except for V4 and V5) lies at the centre of its corresponding image stamp and is marked by a cross-hair.

present the equatorial J2000 celestial coordinates of all of the variable stars discussed in this work. This astrometric solution perfectly agrees with the astrometry given by Stetson (2000) for the standard stars in this cluster.

3. Variable star search strategies

3.1. Standard deviation

V light curves were produced for 1623 stars in the field of our images. The mean magnitude, computed using inverse variance weights, and the rms were calculated for each light curve. Figure 3 shows the rms as a function of the mean magnitude for the V, R, and I filters and indicates the precision of our photometry. Stars with a high dispersion for a given mean magnitude are in principle good candidate variables. However, it is possible that a light curve has a large rms due to occasional poor measurements of the corresponding star in some images, in which case the variability could be spurious.

We used the rms values as a guide to our search for variables. The two known RR Lyrae stars (V1 and V2) and the known red

Table 2. Celestial coordinates for all of the confirmed and candidate variables in our field of view, except V3, which lies outside of our field of view.

ID	type	RA (J2000)	Dec (J2000)	Epoch (days)	P (days)	V (mag)	$V-R$ (mag)	Amp (V) (mag)	Amp(R) (mag)
V1	RR0	23:08:26.68	–15:34:58.5	2 453 949.4046	0.805012	17.303[b]	0.264[b]	0.511	0.408
V2	RR1	23:08:25.00	–15:35:52.9	2 453 284.2652	0.411764[a]	17.256[b]	0.188[b]	0.251	0.140
V4	LPV	23:08:23.19	–15:39:06.0	–	~21.7	14.271[c]	–	~0.18	–
V5	LPV	23:08:39.08	–15:34:36.3	–	–	14.258[c]	–	>0.33	–
V6	SX Phe	23:08:29.16	–15:36:51.1	2 454 318.3687	0.0565500	19.235[b]	0.166[b]	0.136	0.058
V7	SX Phe	23:08:19.83	–15:37:33.6	2 454 839.0479	0.0725859	19.363[b]	0.448[b]	0.050	–
CSX1	SX Phe?	23:08:32.73	–15:35:03.4	–	–	19.499[c]	0.210[c]	~0.15	0.09?

Notes. The coordinates correspond to the epoch of the V reference image, which is the heliocentric Julian date ~2 453 284.26 d. We also include in this table the epoch, period, mean V magnitude, $V-R$ colour, and the full amplitude of each variable. [(a)] If we consider a secular period change, the period is $P_0 = 0.412119$ d at the epoch $E = 2\,453\,284.2652$ d and the period change rate is $\beta \approx 47$ d Myr^{-1}. [(b)] Intensity-weighted magnitude calculated from the light curve model. [(c)] Mean magnitude from our data.

Table 3. Time-series V, R, and I photometry for all of the confirmed and candidate variables in our field of view.

Variable Star ID	Filter	HJD (d)	$M_{\rm std}$ (mag)	$m_{\rm ins}$ (mag)	σ_m (mag)	$f_{\rm ref}$ (ADU s^{-1})	$\sigma_{\rm ref}$ (ADU s^{-1})	$f_{\rm diff}$ (ADU s^{-1})	$\sigma_{\rm diff}$ (ADU s^{-1})	p
V1	V	2 453 283.25245	17.400	18.014	0.009	558.913	0.904	64.366	4.992	1.0059
V1	V	2 453 283.28310	17.444	18.058	0.005	558.913	0.904	39.065	2.618	0.9944
⋮	⋮	⋮	⋮	⋮	⋮	⋮	⋮	⋮	⋮	⋮
V1	R	2 453 283.27903	17.162	17.769	0.004	786.605	0.821	–5.906	3.044	1.0210
V1	R	2 453 283.28689	17.153	17.759	0.004	786.605	0.821	0.832	3.034	1.0184
⋮	⋮	⋮	⋮	⋮	⋮	⋮	⋮	⋮	⋮	⋮
V1	I	2 454 839.03764	16.575	17.636	0.010	865.889	3.651	16.109	8.462	0.9974
V1	I	2 454 839.04150	16.577	17.639	0.007	865.889	3.651	14.141	5.362	0.9945
⋮	⋮	⋮	⋮	⋮	⋮	⋮	⋮	⋮	⋮	⋮

Notes. Note that V3 lies outside of our field of view. The standard $M_{\rm std}$ and instrumental $m_{\rm ins}$ magnitudes are listed in Cols. 4 and 5, respectively, corresponding to the variable star, filter, and heliocentric Julian date of mid-exposure listed in Cols. 1–3, respectively. The uncertainty on $m_{\rm ins}$ is listed in Col. 6, which also corresponds to the uncertainty on $M_{\rm std}$. For completeness, we also list the quantities $f_{\rm ref}$, $f_{\rm diff}$, and p from Eq. (1) in Cols. 7, 9, and 11, along with the uncertainties $\sigma_{\rm ref}$ and $\sigma_{\rm diff}$ in Cols. 8 and 10. This is an extract from the full table, which is available at the CDS.

giant variable (V4) are highlighted with colours as indicated in the caption of Fig. 3. They clearly stand out from the general trend. V3 is not in the field of our images. With this method we also identified another long-period variable discussed later in this paper, which we have labelled V5. While this method is useful for detecting bright variables, it is not useful for detecting shorter-period faint variables in the blue straggler region. It is clear from the red points, which correspond to two new SX Phe and one candidate SX Phe, that they do not stand out in the plot relative to other faint non-variable stars. For these variables, we used a different approach described in the following sections.

3.2. String-length period search

The light curves of the 1623 stars measured in each of the 119 V images were analyzed by the string-length minimization approach (Burke et al. 1970; Dworetsky 1983). In this analysis, the light curve is phased with numerous test periods within a given range. For each period the dispersion parameter S_Q is calculated. When S_Q is at a minimum, the corresponding period produces a phased light curve with a minimum possible dispersion, which is adopted as the best-fit period for that light curve. Bona fide variable stars should have a value of S_Q below a certain threshold. Similar analyses of clusters with numerous variables have shown that all periodic variables with long periods and large amplitudes are likely to have $S_Q \leq 0.3$. However, short-period small-amplitude variables such as SX Phe are often missed by this approach (Arellano Ferro et al. 2004, 2006). Figure 4 shows the distribution of S_Q values for all stars measured in the V images, plotted as a function of an arbitrary star number. We individually explored the light curves below the indicated threshold of $S_Q = 0.3$. With this method we recovered the two RR Lyrae stars in the field of our images (V1 and V2), the LPV V4, and discovered LPV V5. The others stars below this threshold were not found to display true variations.

3.3. Colour–magnitude diagram

The CMD is very useful for separating groups of stars that are potential variables, e.g. in the horizontal branch (HB), the RGB, and the blue straggler region. Figure 5 shows the V versus $(V-R)$ diagram. The known RR0 and RR1 stars contained in our field of view are shown as dark blue and green circles, respectively. The known red giant variable V4 is not shown because it is saturated in our R reference image and V5 is saturated in the R and I reference images. The blue straggler region has been arbitrarily defined with the red box in this CMD. We selected the faint limit such that the photometric uncertainty is below 0.1 mag and the red limit so that the region is not too contaminated by the main sequence.

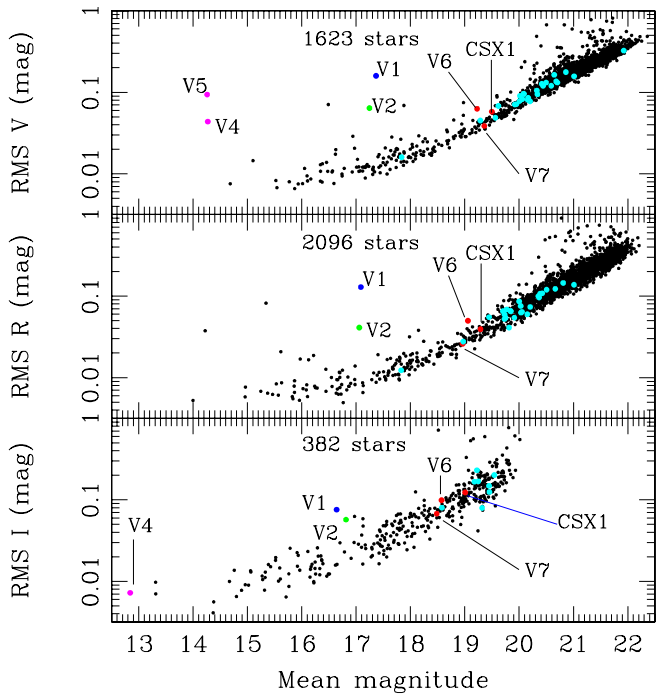

Fig. 3. rms magnitude deviation as a function of the mean magnitude in the filters V, R, and I. Known variables are labelled. V1 (dark blue point) and V2 (green point) are two known RR Lyrae stars in the field of the cluster. Red circles correspond to two newly identified SX Phe stars and one candidate SX Phe. The variable V4 is saturated in our R reference image and the newly identified variable V5 is saturated in the R and I reference images. Hence these stars are not shown in the corresponding plots. The cyan points correspond to the blue stragglers identified by Cote et al. (1991).

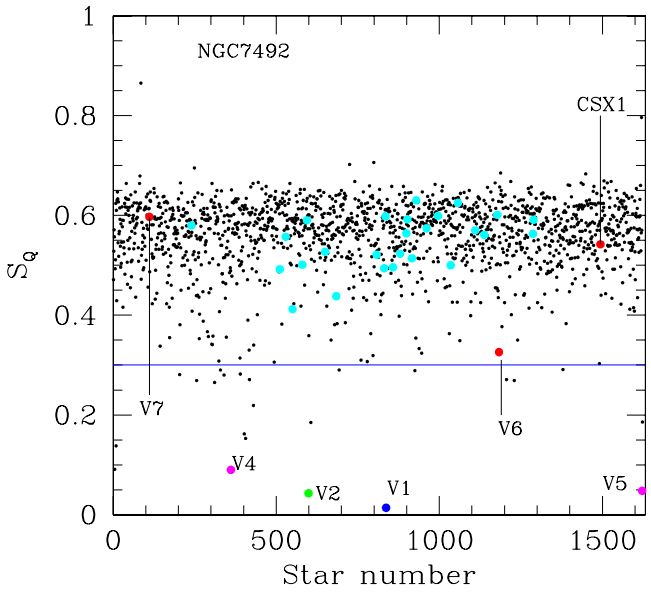

Fig. 4. S_Q values for all stars in the V images as a function of an arbitrary star number. The blue line is the threshold below which RR Lyrae stars tend to be found. The known variables V1, V2, and V4 are labelled as well as the newly identified long-period variable V5, the new SX Phe V6 and V7, and one candidate SX Phe star (red points). The cyan points correspond to the stars identified by Cote et al. (1991) as blue stragglers.

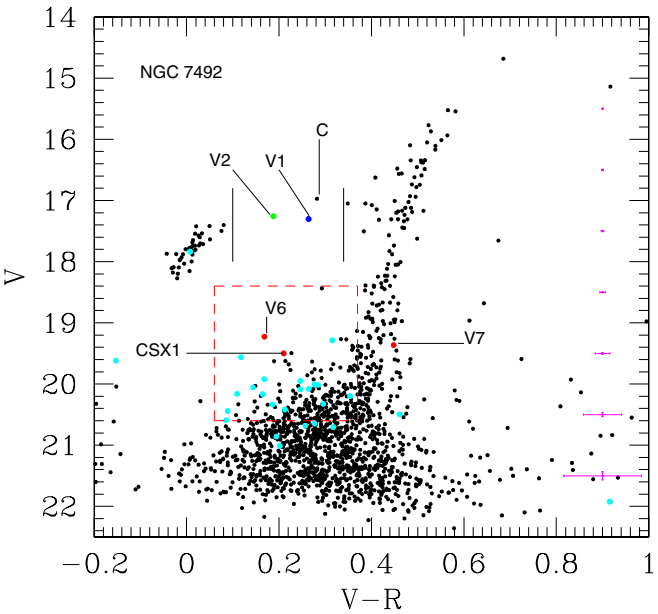

Fig. 5. CMD of NGC 7492. Two known RR Lyrae variables V1 and V2 are marked with dark blue and green symbols, respectively. The new SX Phe variables V6 and V7 and one candidate SX Phe are shown with red symbols. The cyan points correspond to the blue stragglers identified by Cote et al. (1991). The red box is an arbitrarily defined blue straggler region (see text).

It is worth noting that in the HB, the RR Lyrae region is populated only by two of the three previously known RR Lyrae stars and one more star labelled C in the figure. The light curve of star C does not show signs of variation at the precision of our data (~0.02 mag), hence the star may be a field object. Furthermore, there are no saturated stars in the field of view of our V-filter images. Therefore, with a typical precision of ~0.01–0.02 mag in our V light curves at the magnitude of the HB (~17.3 mag), we can be sure that there are no more RR Lyrae stars in the cluster in our field of view (Fig. 2).

3.4. Variability detection statistic $\mathcal{S}_\mathcal{B}$

We also analysed the light curves for variability via the detection statistic $\mathcal{S}_\mathcal{B}$ defined by Arellano Ferro et al. (2012) and employed by these authors to detect amplitude modulations in RR Lyrae stars attributed to the Blazhko effect. The variability detection statistic $\mathcal{S}_\mathcal{B}$ was inspired by the alarm statistic $\mathcal{A}$ defined by Tamuz et al. (2006), designed originally for improving the fitting of eclipsing binary light curves. The advantages of redefining the alarm statistic as

$$S_B = \left(\frac{1}{NM}\right)\sum_{i=1}^{M}\left(\frac{r_{i,1}}{\sigma_{i,1}} + \frac{r_{i,2}}{\sigma_{i,2}} + \ldots + \frac{r_{i,k_i}}{\sigma_{i,k_i}}\right)^2 \quad (3)$$

have been discussed by Arellano Ferro et al. (2012). In this equation, N represents the total number of data points in the light curve and M is the number of groups of time-consecutive residuals of the same sign from a constant-brightness light curve model. The residuals $r_{i,1}$ to r_{i,k_i} form the ith group of k_i time-consecutive residuals of the same sign with corresponding uncertainties $\sigma_{i,1}$ to σ_{i,k_i}. Our $\mathcal{S}_\mathcal{B}$ statistic may therefore be interpreted as a measure of the systematic deviation per data point of the light curve from a non-variable (constant-brightness) model. We note that in Arellano Ferro et al. (2012) the residuals $r_{i,j}$ calculated relative to the Fourier-decomposition light-curve model rather than relative to a constant-brightness model as in this

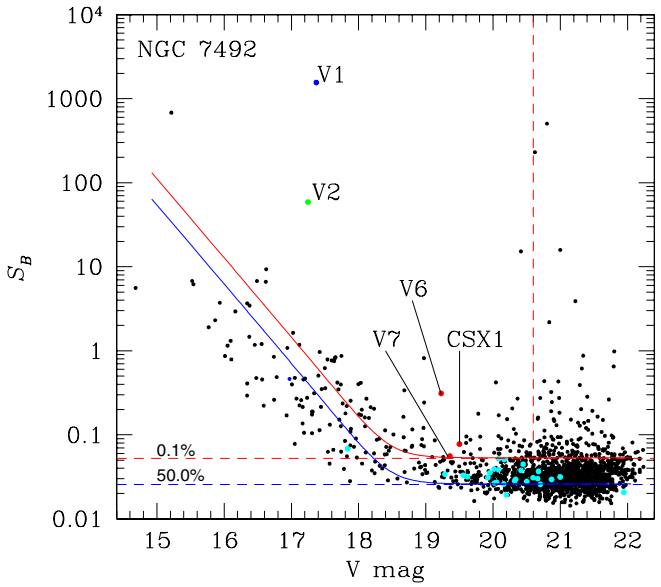

Fig. 6. $\mathcal{S}_{\mathcal{B}}$ statistic as a function of V mean magnitude for the VR combined light curves. The RR Lyrae stars V1 and V2 are labelled, as are the new SX Phe stars V6 and V7 and the one candidate SX Phe star. The cyan points correspond to the blue stragglers identified by Cote et al. (1991). The long-period variables V4 and V5 do not appear on this plot because they are saturated in the R filter. The solid blue curve is the median (50%) curve determined from our simulations and adjusted to fit the real $\mathcal{S}_{\mathcal{B}}$ data above $V \sim 19$ mag. The dashed red curve represents our variable-star detection threshold in $\mathcal{S}_{\mathcal{B}}$ set using our simulations to limit our false-alarm rate to ~0.1%. The solid red curve represents our adopted variable star detection threshold when we take into account the systematic errors. We additionally limited our variable-star search to stars brighter than $V = 20.6$ mag (vertical dashed red line).

work. This difference in application makes $\mathcal{S}_{\mathcal{B}}$ a detection statistic for the Blazhko effect in Arellano Ferro et al. (2012) and a detection statistic for variability in this paper.

Equation (3) was modified from the corresponding equation in Arellano Ferro et al. (2012) by further normalising the $\mathcal{S}_{\mathcal{B}}$ statistic by M. This modification serves to improve the discriminative power of the statistic because variable stars, as opposed to non-variable stars, have longer time-consecutive runs of light curve data points that are brighter or fainter than the constant-brightness model, and therefore have lower values of M (for a given light curve N).

We calculated $\mathcal{S}_{\mathcal{B}}$ for each of our V and R light curves and made plots of $\mathcal{S}_{\mathcal{B}}$ versus magnitude in each filter. The variables detected so far by the methods discussed in Sects. 3.1–3.3 (V1, V2, V4 and V5) stand out in these diagrams with very high $\mathcal{S}_{\mathcal{B}}$ values compared with the other stars. However, we found that we could make these differences in the $\mathcal{S}_{\mathcal{B}}$ values between variable and non-variable stars even larger by calculating $\mathcal{S}_{\mathcal{B}}$ for the combined VR light curves. In this case, we adjusted the R light curve for each star so that its mean magnitude matched that of the corresponding V light curve and then calculated $\mathcal{S}_{\mathcal{B}}$ for the combined VR light curve[3].

In Fig. 6 we plot $\mathcal{S}_{\mathcal{B}}$ for each of the combined VR light curves as a function of the V mean magnitude. The RR Lyrae stars V1 and V2 clearly have $\mathcal{S}_{\mathcal{B}}$ values among the highest in the light curve sample. It is interesting to note that $\mathcal{S}_{\mathcal{B}}$ generally scatters around a constant value (~0.03) for V fainter than ~19 mag. For stars brighter than $V \sim 19$ mag, the $\mathcal{S}_{\mathcal{B}}$ values show an exponential increase (which appears as linear on the log-scale of Fig. 6). This feature can be explained by considering the systematic errors that exist at some level in all light curves. However, we defer the relevant dicussion of this topic to a later point in this section.

To detect new variable stars, we need to define a detection threshold that optimises our sensitivity to real variables while being set high enough to minimise the number of false alarms (i.e. classification of non-variable stars as variable). Without setting this detection threshold carefully, one runs the risk of publishing suspected variable stars of which the majority may be refuted in subsequent photometric campaigns (see Safonova & Stalin 2011 and Bramich et al. 2012 for a good example). We decided to determine the threshold for our $\mathcal{S}_{\mathcal{B}}$ statistic with simulations.

For each combined VR light curve in our sample, we performed 10^6 simulations. Each simulation consists of generating a random light curve m_i using the real light-curve data-point uncertainties σ_i via

$$m_i = \overline{V} + \lambda_i \sigma_i, \tag{4}$$

where the λ_i are a set of random deviates drawn from a normal distribution with zero mean and unit σ, and $\overline{V}$ is the mean V magnitude of the real light curve. We calculated $\mathcal{S}_{\mathcal{B}}$ for the simulated light curves and obtained a distribution of 10^6 $\mathcal{S}_{\mathcal{B}}$ values from which we determined the median (50%) and 99.9% percentile.

We found that the median values of the $\mathcal{S}_{\mathcal{B}}$ distributions are approximately the same (to within the noise of the finite number of simulations) for all of our stars, as are the 99.9% percentile values, which implies that for light curves with the same number of data points, the actual distribution of data point uncertainties has no impact on the threshold to be chosen for $\mathcal{S}_{\mathcal{B}}$. We found that for our combined VR light curves, the mean of the $\mathcal{S}_{\mathcal{B}}$ distribution medians is ~0.0256, and the mean of the 99.9% percentiles is ~0.0525. These lines are plotted in Fig. 6 as the horizontal dashed blue and red lines.

Looking again at Fig. 6, we now see that the $\mathcal{S}_{\mathcal{B}}$ values for the real light curves scatter close to the median line from the simulations for stars fainter than $V \sim 19$ mag, which implies that for these stars the simulations provide a reasonably good model for the noise in the real light curves. However, for stars brighter than $V \sim 19$ mag, the $\mathcal{S}_{\mathcal{B}}$ values for the real light curves increase exponentially with increasing brightness and are much higher than we would expect as determined from our light curve simulations with pure Gaussian noise. We can explain this by considering that the systematic errors in the light curves, which correlate over groups of time-consecutive data points and therefore mimic real variability, increasingly dominate the noise in our real light curves with increasing star brightness. To account for the systematic errors, we need to adjust our median and 99.9% percentile curves in Fig. 6, which we do by fitting a linear relation to the log-$\mathcal{S}_{\mathcal{B}}$ values for V brighter than 19 mag and merging this fit with the constant median curve for V fainter than 19 mag (solid blue curve). We then shift this curve to higher $\mathcal{S}_{\mathcal{B}}$ values so that the horizontal part matches that of the 99.9% percentile (solid red curve). Finally we adopt the solid red curve as our detection threshold for new variables.

By choosing a variable star detection threshold set to the 99.9% percentile of $\mathcal{S}_{\mathcal{B}}$ from our simulations of light curves that have only pure Gaussian noise, we have set our false alarm rate to 0.1%, which implies that with 1585 stars with combined VR light curves we should expect only ~1.6 non-variable stars to

[3] This procedure is valid for the variable stars in our data because the data points in our light curves generally alternate between the two filters and therefore the light curve data in each filter have approximately the same phase coverage.

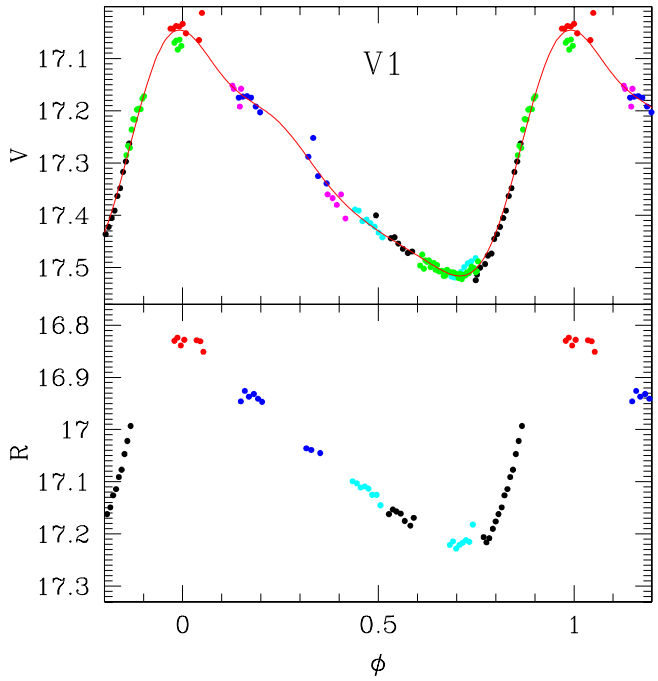

Fig. 7. Light curve of the RR0 star V1 in the *V* filter (*top*) and the *R* filter (*bottom*) phased with the period 0.805012 d. The data point colours represent the different epochs listed in Table 5. The red line corresponds to the Fourier fit of Eq. (3) with four harmonics. The typical uncertainties in the *V* and *R* magnitudes are ∼0.007 and 0.005 mag, respectively.

fall above our threshold. However, since we are fully aware that the systematic errors may affect some light curves more than others for various reasons (e.g. near a saturated star, cosmic ray hits, etc.), we must still exercise caution with all candidate variable stars that lie above our detection threshold in $\mathcal{S}_{\mathcal{B}}$. We observe that for stars fainter than $V = 20.6$ mag, the $\mathcal{S}_{\mathcal{B}}$ values have a larger number of high outliers than is typical and therefore we further limit our variable star search to stars brighter than $V = 20.6$ mag (vertical dashed red line in Fig. 6). We note that the two RR Lyrae stars V1 and V2 have $\mathcal{S}_{\mathcal{B}}$ values much greater than our adopted detection threshold and are therefore recovered by this method.

We explored the appearance of the light curves of all stars with $\mathcal{S}_{\mathcal{B}}$ above our detection threshold and found convincing indications of variability in two stars in the blue straggler region. These SX Phe stars are discussed in Sect. 6 along with one other candidate SX Phe star that also lies above our detection threshold in $\mathcal{S}_{\mathcal{B}}$. The remaining stars with $\mathcal{S}_{\mathcal{B}}$ values above our threshold do not show convincing light curve variability either on inspection of their light curves or when analysed with the string-length minimisation approach.

If we compare this method with the others used in this paper for detecting variable stars (see Sects. 3.1, 3.2), it becomes clear that this method is the only one that has been used to successfully detect all of the previously known and new variables in this cluster.

4. RR Lyrae stars

Of the three known RR Lyrae stars in the cluster, the RR1 star V3 is not in the field of our images.

V1. This is a clear fundamental-mode pulsator or RR0. Our data are neatly phased with a period of 0.805012 d (Fig. 7). The light curve was fitted with four Fourier harmonics (red continuous line in Fig. 7) of the form of Eq. (5).

$$m(t) = A_{\rm o} + \sum_{k=1}^{N} A_k \cos\left(\frac{2\pi}{P}\, k\,(t-E) + \phi_k\right). \quad (5)$$

We noted that using more than four harmonics results in overfitting. The decomposition of the light curve in Fourier harmonics was used to estimate the iron abundance [Fe/H] and the absolute magnitude M_V, and hence the distance. These calculations were made using the semi-empirical calibrations available in the literature.

To calculate [Fe/H] we employed the calibration of Jurcsik & Kovacs (1996) valid for RR0 stars.

$$[{\rm Fe/H}]_J = -5.038 - 5.394\,P + 1.345\,\phi_{31}^{(s)}. \quad (6)$$

The Fourier parameter $\phi_{31}^{(s)}$ comes from fitting a sine series to the light curve of star V1 rather than a cosine series, as in Eq. (5). However, the corresponding cosine parameter $\phi_{31}^{(c)}$ is related by $\phi_{31}^{(s)} = \phi_{31}^{(c)} - \pi$. This equation gives $[{\rm Fe/H}]_J$ with a standard deviation from this calibration of 0.14 dex (Jurcsik 1998). The Jurcsik metallicity scale can be transformed to the Zinn & West (1984) scale $[{\rm Fe/H}]_{\rm ZW}$ through the relation $[{\rm Fe/H}]_J = 1.43\,[{\rm Fe/H}]_{\rm ZW} + 0.88$ (Jurcsik 1995). We note that the deviation parameter *Dm* (Jurcsik & Kovacs 1996) for this star when fitting higher-order Fourier series is greater than the recommended value. Hence, our metallicity estimate should be treated with caution.

We also calculated the metallicity on the UVES scale using the equation of Carretta et al. (2009):

$$[{\rm Fe/H}]_{\rm UVES} = -0.413 + 0.130[{\rm Fe/H}]_{\rm ZW} - 0.356[{\rm Fe/H}]^2_{\rm ZW}. \quad (7)$$

From our light curve fit, we find $\phi_{31}^{(c)} = 8.987$ and obtain $[{\rm Fe/H}]_{\rm ZW} = -1.68 \pm 0.10$ or $[{\rm Fe/H}]_{\rm UVES} = -1.64 \pm 0.13$. These metallicity values agree well with the mean spectroscopic values of $[{\rm Fe/H}] = -1.82 \pm 0.05$ and $[{\rm Fe/H}] = -1.79 \pm 0.06$ determined by Cohen & Melendez (2005) from Fe I and Fe II lines, respectively, in four bright red giants in the cluster. The Fe abundances were derived using high-resolution ($R = \lambda/\delta\lambda = 35\,000$) spectra obtained with HIRES at the Keck Observatory. Similarly they agree well with the latest spectroscopic metallicities from Saviane et al. (2012) (see Table 4).

Other metallicity estimates for this cluster are $[{\rm Fe/H}] = -1.70 \pm 0.06$ from Rutledge et al. (1997) determined using moderate dispersion spectroscopy in the region of the infrared Ca triplet, $[{\rm Fe/H}] = -1.5 \pm 0.3$ from Zinn & West (1984) using the narrow-band Q39 photometric system, and $[{\rm Fe/H}] = -1.34 \pm 0.25$ by Smith (1984) using the ΔS method for two RR Lyraes in the cluster. Thus the metallicity estimated via the Fourier decomposition technique agrees well with the other independent estimates (see Table 4).

To determine of the absolute magnitude of V1 we employed the calibration of Kovács & Walker (2001),

$$M_V = -1.876\,\log P - 1.158\,A_1 + 0.821\,A_3 + K, \quad (8)$$

which has a standard deviation of 0.04 mag. From our fit of Eq. (5) to the light curve of V1, we derive $A_1 = 0.206$ and $A_3 = 0.034$ mag. We adopted $K = 0.41$ mag to be consistent with a true distance modulus for the Large Magellanic Cloud (LMC) of $\mu_0 = 18.5$ mag (see the discussion in Arellano Ferro et al. 2010, in their Sect. 4.2). We obtain $M_V = 0.376 \pm 0.040$ mag, which is equivalent to the luminosity $\log(L/L_\odot) = 1.762 \pm 0.016$.

Table 4. Metallicity estimates for NGC 7492 on the ZW scale and their respective values on the UVES scale and vice versa, as found from the literature search.

$[Fe/H]_{ZW}$	$[Fe/H]_{UVES}$	Reference	Method
-1.68 ± 0.10	-1.64 ± 0.13^c	This work	Fourier light-curve decomposition of the RR Lyrae stars
	-1.72 ± 0.07	Saviane et al. (2012)	Ca_{II} triplet using the FORS2 imager and spectrograph at the VLT
	-1.69 ± 0.08	Saviane et al. (2012)	Ca_{II} triplet using the FORS2 imager and spectrograph at the VLT
	-1.69 ± 0.08	Carretta et al. (2009)	Weighted average of several metallicities[b]
-1.82 ± 0.05	-1.83 ± 0.07^c	Cohen & Melendez (2005)	Fe_I line in bright red giants in this cluster
-1.79 ± 0.06	-1.79 ± 0.08^c	Cohen & Melendez (2005)	Fe_{II} line in bright red giants in this cluster
-1.70 ± 0.06	-1.66 ± 0.08^c	Rutledge et al. (1997)	Infrared Ca triplet
	-1.78	Harris (1996)	Globular cluster catalogue[a]
-1.5 ± 0.3	-1.41 ± 0.36^c	Zinn & West (1984)	Narrow band Q39 photometric system
-1.34 ± 0.25	-1.23 ± 0.27^c	Smith (1984)	ΔS method for two RR Lyraes in the cluster

Notes. [(a)] The catalogue version used is the updated 2010 version available at `http://www.physics.mcmaster.ca/Globular.html`. [(b)] Carretta et al. (2009); Carretta & Gratton (1997); Kraft & Ivans (2003), and the recalibration of the Q39 and W″ indices. [(c)] Converted from Col. 1 using Eq. (7) (Carretta et al. 2009).

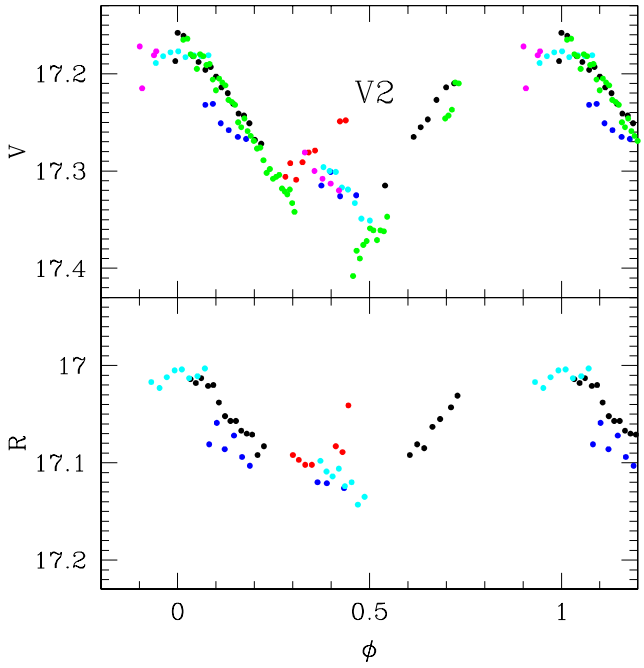

Fig. 8. Light curve of the RR1 star V2 in the *V* filter (*top*) and the *R* filter (*bottom*) phased with the period 0.411764 d. The data point colours represent the different epochs listed in Table 5. The typical uncertainties in the *V* and *R* magnitudes are ~0.007 and 0.005 mag, respectively.

Assuming $E(B-V) = 0.0$ mag (Harris 1996), the true distance modulus is $\mu_0 = 16.927 \pm 0.040$ mag, equivalent to a distance of 24.3 ± 0.5 kpc. Cote et al. (1991) estimated a distance of 26.18 ± 2.41 kpc to NGC 7492 using the cluster NGC 6752 as a reference, whose distance was estimated by Penny & Dickens (1986). Our distance estimate using V1 agrees within the uncertainties.

V2. This RR1 star shows a complex light curve. The period derived by Barnes (1968) of 0.292045 d fails to phase our light curve properly. Using the string-length minimisation method on our light curve, we determine a period of 0.411764 d, which produces the phased light curve shown in Fig. 8. The period is towards the upper limit for an RR1 type star. However, long periods like this are not uncommon in Oosterhoff type II clusters, which typically have a similar metallicity and horizontal branch morphology as NGC 7492 (Lee 1990; Clement et al. 2001). We note that our light curve does not phase well at this period and so we searched for a second period. As the ratio $P_1/P_0 = 0.746 \pm 0.001$ (Catelan 2009; Cox et al. 1983) in RRd stars, we expect the second period to be ~0.5519 d when performing a search of the residuals from the first period. We could only find a non-significant second period with $P_1 = 0.4365$ d. The light curve shows nightly amplitude changes that resemble those found by Arellano Ferro et al. (2012) in the majority of RR1 stars in NGC 5024.

We attempted to model the light curve with a secular period change, which we parameterised as in Bramich et al. (2011), i.e.

$$\phi(t) = \frac{t-E}{P(t)} - \left\lfloor \frac{t-E}{P(t)} \right\rfloor \quad (9)$$

$$P(t) = P_0 + \beta(t-E), \quad (10)$$

where ϕ(t) is the phase at time t, $P(t)$ is the period at time t, P_0 is the period at the epoch E, and β is the rate of period change. We searched the parameter space at fixed epoch E, whose value is arbitrary, for the best-fitting values of P_0 and β, using as a criterion the minimum string-length statistic of the light curve. The search was conducted in a small range of periods around the previously determined best-fitting period. This is the only type of period change that we can consider modelling given our limited photometric data.

We found a period of $P_0 = 0.412119$ d at the epoch $E = 2\,453\,284.2652$ d and a period change rate of $\beta \approx 47$ d Myr^{-1}. The light curve phased with ϕ(t) from Eq. (9) is shown in Fig. 9. Clearly, the phased light curve is now much improved, but we still observe possible amplitude modulations, which may be due to the Blazhko effect. This period change rate is higher than other values found in the literature by a factor of two or more (Le Borgne et al. 2007; Lee 1991; Jurcsik et al. 2001), but given our limited data we cannot speculate on the cause.

5. Long-period variables

V4. This red giant variable, discovered by Barnes (1968), clearly stands out as a variable in Figs. 3 and 4. Barnes (1968) estimated a period of 17.9 days but pointed out that the observations did not cover the whole period. Our data set for this star consists of 119 *V* filter epochs distributed over a baseline of eight years (top panel of Fig. 10). Thus our data are less than ideal for estimating an accurate period. Nevertheless, using the `Period04` program (Lenz & Breger 2005), we find a period of ~21.7 d. In the *V* vs. $(V-I)$ diagram (not plotted in the paper), the star is situated in

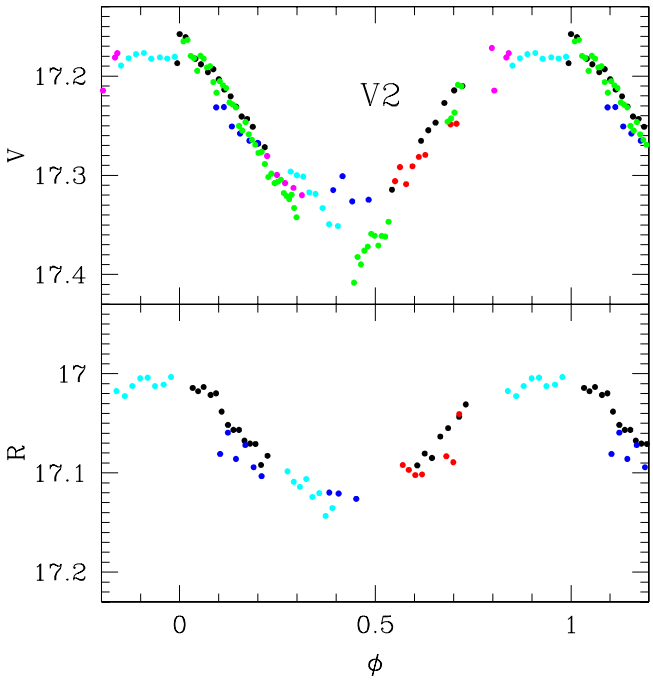

Fig. 9. Same as Fig. 8, except that now the light curve of V2 is phased with the period $P_0 = 0.412119$ d at the epoch $E = 2\,453\,284.2652$ d with an ephemeris that includes a period change rate $\beta \approx 47$ d Myr^{-1}.

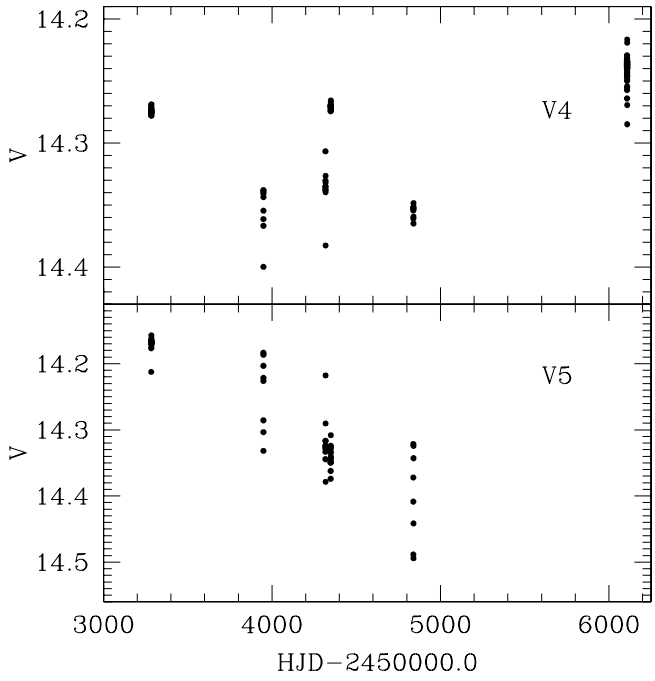

Fig. 10. Light curves of the variables V4 and V5 in the V filter.

Table 5. Data point colours used to mark different observing runs in Figs. 7, 8, 9, 11 and 12.

Dates	Colour
20041004–20041005	Black
20060801	Red
20070804–20070805	Blue
20070904–20070905	Cyan
20090107–20090108	Magenta
20120628–20120629	Green

the upper region of the red giant branch. Exploring the Catalogue of Variable Stars in Galactic Globular Clusters (Clement et al. 2001), one finds LBs (slow irregular variables of types K, M, C, and S; see the General Catalog of Variable Stars (Kholopov et al. 1996) for classifications of variables) with periods of 13–20 d and amplitudes 0.1–0.4 mag. See for example V8 and V10 in NGC 2419. See also V109 in NGC 5024 which is listed as a semi-regular variable with a period of 21.93 d and amplitude of 0.05 mag. Our data for V4 are consistent with the classification as a long-period variable.

V5. From Figs. 3 and 4 we discovered this new long-period variable. Its light curve is shown in the bottom panel of Fig. 10. This star is saturated in our R and I images and hence we have not been able to plot it in the CMD and determine its classification (e.g. as a red giant). It is evident from the light curve that the star undergoes a long-term dimming.

We note that for both V4 and V5, the formal uncertainties on the data points are typically ~0.001 mag. However, these stars are very bright and their light curves suffer from systematic errors that correlate during the nightly observations, leading to a relatively large intra-night scatter (see Fig. 10).

6. SX Phoenicis stars and candidates

We have discovered two new SX Phe stars, which we label V6 and V7, and one candidate SX Phe star, which we label CSX1.

V6. This variable was found above our detection threshold for the $\mathcal{S}_{\mathcal{B}}$ statistic in Sect. 3.4 (see Fig. 6). In the CMD it is placed well inside the blue straggler region (see Fig. 5). In fact, this star is a blue straggler found by Cote et al. (1991). We analysed the V light curve with `Period04` and found a clear frequency at 17.683477 cycles d^{-1} (or a period of 0.0565500 d). We found no other significant frequencies. Based on the blue straggler status and the detected period, we can be sure that this is an SX Phe star.

In Fig. 11, we present the phased light curve in the V and R filters. We overplot the best-fit sine curve as a solid black line. As expected, the R filter light curve shows variations with the same period and phase as the V filter light curve, but with smaller amplitude. There is a hint that the amplitude of V6 changed between different observing runs (compare the black points from 2004 with the green points from 2012). There are previous studies about SX Phe stars that show a period as well as an amplitude change. See for example Fig. 25 and Sect. 4.2 in Nemec et al. (1995) and also Sect. 5.2 in Arellano Ferro et al. (2010).

SX Phe stars are well known as distance indicators through their P-L relation (e.g. Jeon et al. 2003). By adopting the P-L relation for the fundamental mode recently calculated by Cohen & Sarajedini (2012) for a sample of 77 double-mode SX Phe stars in Galactic globular clusters, which is of the form $M_V = -1.640(\pm0.110) - 3.389(\pm0.090)\log(P_f)$, we can calculate $M_V = 2.588 \pm 0.157$ mag for V6 assuming that it is pulsating in the fundamental mode. Given this, and assuming $E(B-V) = 0.0$ mag, we obtain a true distance modulus $\mu_0 = 16.644 \pm 0.157$ mag, which translates to a distance of $\sim 21.3 \pm 1.5$ kpc. Hence, if V6 is pulsating in the fundamental mode, it cannot be a cluster member.

However, if we assume that V6 is pulsating in the first overtone (1H), we may "fundamentalise" the detected frequency by multiplying it by the frequency ratio $f_1/f_2 = 0.783$ (see

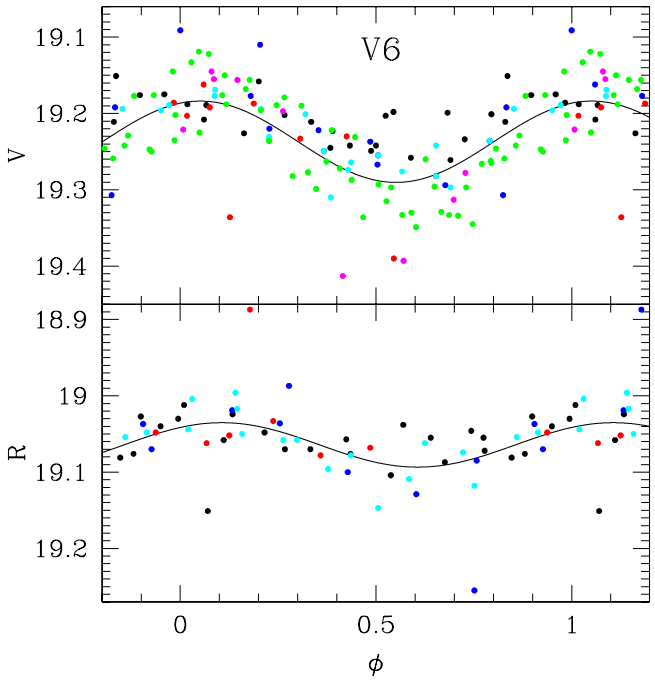

Fig. 11. Light curve of the newly discovered SX Phe star V6 in the *V* filter (*top*) and *R* filter (*bottom*) phased with the period 0.0565500 d. The data point colours represent the different epochs listed in Table 5. The solid black curves represent the best-fit sine curves at the phasing period. The typical uncertainties in the *V* and *R* magnitudes are ~0.02 mag.

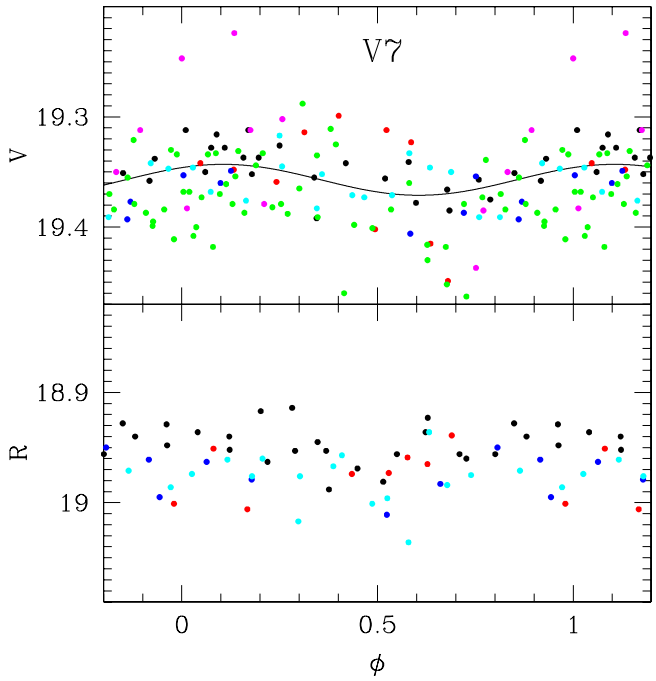

Fig. 12. Light curve of the newly discovered SX Phe star V7 in the *V* filter (*top*) and *R* filter (*bottom*) phased with the period 0.0725859 d. The data point colours represent the different epochs listed in Table 5. The solid black curve represents the best-fit sine curve at the phasing period in the *V* filter. The typical uncertainties in the *V* and *R* magnitudes are ~0.02 mag.

Santolamazza et al. 2001; Jeon et al. 2003; Poretti et al. 2005). Using the Cohen & Sarajedini (2012) P-L relation as before, we obtain $M_V = 2.228 \pm 0.149$ mag, $\mu_0 = 17.004 \pm 0.149$ mag, and a distance of $\sim 25.2 \pm 1.8$ kpc. Hence, if V6 is pulsating in the first overtone, it is most likely a cluster member.

Unfortunately, without detecting two frequencies in the light curve of V6, we cannot further speculate on the pulsation mode of this star.

V7. Again, this variable was found above our detection threshold for the $\mathcal{S}_{\mathcal{B}}$ statistic. In the CMD, it lies on the RGB at the edge of the blue straggler region. We analysed the *V* light curve with `Period04` and found a candidate frequency at 13.776775 cycles d^{-1} (or a period of 0.072586 d). We found no other significant frequencies.

In Fig. 12, we present the phased light curve in the *V* and *R* filters along with the best-fit sine curve in *V* (solid black curve). The variations at an amplitude of ~0.05 mag are barely visible in the phased *V* light curve. To quantify our classification of V7 as a variable with the detected period, we calculated the improvement in chi-squared $\Delta\chi^2$ when fitting the sine curve compared with a constant magnitude. Under the null hypothesis that the light curve is not variable, the $\Delta\chi^2$ statistic follows a chi-squared distribution with two degrees of freedom. We set our threshold for rejection of the null hypothesis at 1%, which is equivalent to $\Delta\chi^2 \gtrsim 9.21$. The *V* light curve of V7 has $\Delta\chi^2 \approx 14.40$, which supports our conclusion that it is variable. We note that the light curve is not detected as showing variability by the $\Delta\chi^2$ test in the *R* filter.

Using the Cohen & Sarajedini (2012) P-L relation for the detected frequency, we obtain $M_V = 2.221 \pm 0.152$ mag, $\mu_0 = 17.142 \pm 0.152$ mag, and a distance of $\sim 26.8 \pm 1.8$ kpc, which is consistent with the distance to the cluster. Considering all the evidence we have discussed, we classify this star as an SX Phe star that is most likely a cluster member pulsating in the fundamental mode.

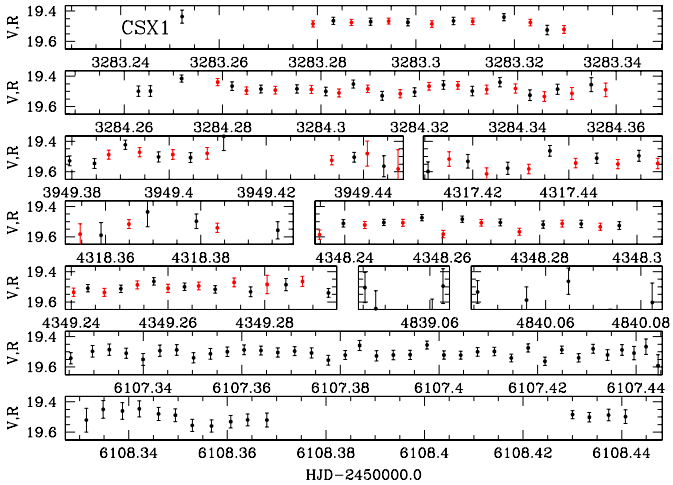

Fig. 13. Light curve of the candidate SX Phe star CSX1. Black points correspond to the *V* magnitudes and red points correspond to the *R* magnitudes (which are shifted in mean magnitude to match the mean magnitude of the *V* data). Some data points fall outside of the plot magnitude range.

CSX1. This star was detected above the threshold for the $\mathcal{S}_{\mathcal{B}}$ statistic lies in the blue straggler region in the CMD. We searched for frequencies in the *V* light curve using `period04`, but found no clear peaks. However, on our inspection of the light curve on individual nights, we found clear cyclical variations on time scale of ~1 h (see Fig. 13). Since we were unable to detect a pulsation frequency, we classify this star as a candidate SX Phe for which follow-up observations would be desirable.

Table 6. Detected pulsation frequencies for the new SX Phe variables discovered in NGC 7492.

ID	$A_0{}^a$ (V mag)	Label	Frequency (c/d^{-1})	$A_V{}^b$ (mag)	Mode
V6	19.235(4)	f_1	17.683477(13)	0.123(10)	$1H?^c$
V7	19.363(4)	f_1	13.776775(32)	0.030(10)	$F?^c$

Notes. The numbers in parenthesis indicate the uncertainty on the last decimal place. [(a)] Mean V magnitude A_0. [(b)] Full amplitude A_V in the V filter. [(c)] If we assume that these stars are cluster members, they are likely to be pulsating in the suggested mode.

Periods and amplitudes for the two new SX Phe and one candidate are given in Table 6. They are also labelled in the CMD in Fig. 5 and their equatorial coordinates (J2000) are listed in Table 2. We note that the $(V-R)$ colours of V6 and V7, converted to $(B-V)$ using the colour transformations of VandenBerg & Clem (2003), are consistent (within 1σ) with the $(B-V)$ colour-period relation of McNamara (2011).

7. Conclusions

Precise time series differential CCD V, R, I photometry with a baseline of about eight years has been performed to detect brightness variations in stars with $14.0 < V < 19.5$ mag in the field of NGC 7492. We found the following:

1. We identified one new long-period variable (V5) and two SX Phe stars (V6 and V7). We presented one candidate SX Phe (CSX1), which requires more high-precision data to finally establish its nature.
2. With the $\mathcal{S}_\mathcal{B}$ variability statistic, it was possible to recover all previously known variables and also to find the new variables presented in this work.
3. Our photometric precision at the magnitude of the horizontal branch combined with the consideration of the CMD means that we can be sure that there are no undetected RR Lyrae stars that are cluster members in the field of view of our images.
4. We improved the period estimate for the RR0 star V1, and performed a Fourier analysis to estimate a cluster metallicity of $[\mathrm{Fe/H}]_{\mathrm{ZW}} = -1.68 \pm 0.10$ or $[\mathrm{Fe/H}]_{\mathrm{UVES}} = -1.64 \pm 0.13$ and a distance of $\sim 24.3 \pm 0.5$ kpc.
5. We found that the RR1 star V2 is undergoing a period change at a rate of $\beta \approx 47$ d Myr^{-1}. We also found tentative evidence for the presence of the Blazhko effect in the light curve.
6. By assuming that the SX Phe stars are cluster members (which is consistent with their position in the CMD), we used the SX Phe P-L relation to speculate on the mode of oscillation of each star. We also obtained independent distance estimates to the cluster of $\sim 25.2 \pm 1.8$ and 26.8 ± 1.8 kpc.
7. The cluster metallicity and distance estimates that we derived in this paper are all consistent with previous estimates in the literature.

Acknowledgements. A.A.F. acknowledges financial support from DGAPA-UNAM grant through project IN104612. We are thankful to the CONACyT (México) and the Department of Science and Technology (India) for financial support under the Indo-Mexican collaborative project DST/INT/MEXICO/RP001/2001. We thank the staff at IAO and at the remote-control station at CREST, Hosakote for assistance during the observations. This work has made use of the SIMBAD and ADS services, for which we are thankful.

References

Arellano Ferro, A., Arévalo, M. J., Lázaro, C., et al. 2004, Rev. Mex. Astron. Astrofis., 40, 209
Arellano Ferro, A., García Lugo, G., & Rosenzweig, P. 2006, Rev. Mex. Astron. Astrofis., 42, 75
Arellano Ferro, A., Giridhar, S., & Bramich, D. M. 2010, MNRAS, 402, 226
Arellano Ferro, A., Figuera Jaimes, R., Giridhar, S., et al. 2011, MNRAS, 416, 2265
Arellano Ferro, A., Bramich, D. M., Figuera Jaimes, R., Giridhar, S., & Kuppuswamy, K. 2012, MNRAS, 420, 1333
Barnes, S. A. 1968, AJ, 73, 579
Bramich, D. M. 2008, MNRAS, 386, L77
Bramich, D. M., Figuera Jaimes, R., Giridhar, S., & Arellano Ferro, A. 2011, MNRAS, 413, 1275
Bramich, D. M., Arellano Ferro, A., Jaimes, R. F., & Giridhar, S. 2012, MNRAS, 424, 2722
Bramich, D. M., Horne, K., Albrow, M. D., et al. 2013, MNRAS, 428, 2275
Buonanno, R., Corsi, C. E., Ferraro, I., & Fusi Pecci, F. 1987, A&AS, 67, 327
Burke, E. W., Jr., Rolland, W. W., & Boy, W. R. 1970, JRASC, 64, 353
Carretta, E., & Gratton, R. G. 1997, A&AS, 121, 95
Carretta, E., Bragaglia, A., Gratton, R., D'Orazi, V., & Lucatello, S. 2009, A&A, 508, 695
Catelan, M. 2009, Ap&SS, 320, 261
Clement, C. M., Muzzin, A., Dufton, Q., et al. 2001, AJ, 122, 2587
Cohen, J. G., & Melendez, J. 2005, AJ, 129, 1607
Cohen, R. E., & Sarajedini, A. 2012, MNRAS, 419, 342
Corwin, T. M., Sumerel, A. N., Pritzl, B. J., et al. 2006, AJ, 132, 1014
Cote, P., Richer, H. B., & Fahlman, G. G. 1991, AJ, 102, 1358
Cox, A. N., Hodson, S. W., & Clancy, S. P. 1983, ApJ, 266, 94
Draper, P. W. 2000, Astronomical Data Analysis Software and Systems IX, 216, 615
Dworetsky, M. M. 1983, MNRAS, 203, 917
Harris, W. E. 1996, VizieR Online Data Catalog, VII/195
Jeon, Y.-B., Lee, M. G., Kim, S.-L., & Lee, H. 2003, AJ, 125, 3165
Jurcsik, J. 1995, Acta Astron., 45, 653
Jurcsik, J. 1998, A&A, 333, 571
Jurcsik, J., & Kovacs, G. 1996, A&A, 312, 111
Jurcsik, J., Clement, C., Geyer, E. H., & Domsa, I. 2001, AJ, 121, 951
Kains, N., Bramich, D. M., Figuera Jaimes, R., et al. 2012, A&A, 548, A92
Kholopov, P. N., Samus', N. N., Frolov, M. S., et al. 1996, VizieR Online Data Catalog, II/139
Kovács, G., & Walker, A. R. 2001, A&A, 371, 579
Kraft, R. P., & Ivans, I. I. 2003, PASP, 115, 143
Landolt, A. U. 1992, AJ, 104, 340
Le Borgne, J. F., Paschke, A., Vandenbroere, J., et al. 2007, A&A, 476, 307
Lee, Y.-W. 1990, ApJ, 363, 159
Lee, Y.-W. 1991, ApJ, 367, 524
Lenz, P., & Breger, M. 2005, Comm. Asteroseismol., 146, 53
McNamara, D. H. 2011, AJ, 142, 110
Nemec, J. M., Mateo, M., Burke, M., & Olszewski, E. W. 1995, AJ, 110, 1186
Penny, A. J., & Dickens, R. J. 1986, MNRAS, 220, 845
Poretti, E., Suárez, J. C., Niarchos, P. G., et al. 2005, A&A, 440, 1097
Rutledge, G. A., Hesser, J. E., & Stetson, P. B. 1997, PASP, 109, 907
Safonova, M., & Stalin, C. S. 2011, AJ, 142, 179
Santolamazza, P., Marconi, M., Bono, G., et al. 2001, ApJ, 554, 1124
Saviane, I., da Costa, G. S., Held, E. V., et al. 2012, A&A, 540, A27
Shapley, H. 1920, ApJ, 52, 73
Smith, H. A. 1984, ApJ, 281, 148
Stetson, P. B. 2000, PASP, 112, 925
Strader, J., Everitt, H. O., & Danford, S. 2002, MNRAS, 335, 621
Tamuz, O., Mazeh, T., & North, P. 2006, MNRAS, 367, 1521
VandenBerg, D. A., & Clem, J. L. 2003, AJ, 126, 778
Zacharias, N., Finch, C., Girard, T., et al. 2010, AJ, 139, 2184
Zinn, R., & West, M. J. 1984, ApJS, 55, 45